Earth's Future

RESEARCH ARTICLE
10.1029/2024EF005003

Wetland Gain and Loss in the Mississippi River Bird-Foot Delta

Jiangjie Yang[1], Zhijun Dai[1,2], Xuefei Mei[1], Yaying Lou[3], and Sergio Fagherazzi[4]

[1]State Key Laboratory of Estuarine and Coastal Research, East China Normal University, Shanghai, China, [2]Laboratory for Marine Geology, Qingdao Marine Science and Technology Center, Qingdao, China, [3]Zhuhai-M.U.S.T. Science and Technology Research Institute, Zhuhai, China, [4]Department of Earth and Environment, Boston University, Boston, MA, USA

Key Points:

- The land of Mississippi River Bird-Foot Delta didn't experience holistic shoreline retreat
- Lateral erosion of the eastern and southeastern shorelines was determined by the persistent action of the ENE to SSE waves
- The narrowing of the Main Pass and Pass a Loutre is responsible for hindrance the transport of water and sediment into the deltaic margins

Supporting Information:

Supporting Information may be found in the online version of this article.

Correspondence to:

Z. Dai, and Y. Lou,
zjdai@sklec.ecnu.edu.cn;
zumri.allisonl@um.edu.mo

Citation:

Yang, J., Dai, Z., Mei, X., Lou, Y., & Fagherazzi, S. (2025). Wetland gain and loss in the Mississippi River bird-foot delta. *Earth's Future*, *13*, e2024EF005003. https://doi.org/10.1029/2024EF005003

Received 19 JUN 2024
Accepted 26 MAY 2025

Author Contributions:

Conceptualization: Zhijun Dai
Data curation: Jiangjie Yang, Zhijun Dai, Yaying Lou
Formal analysis: Jiangjie Yang, Zhijun Dai, Xuefei Mei, Yaying Lou
Funding acquisition: Zhijun Dai
Investigation: Jiangjie Yang, Zhijun Dai, Xuefei Mei, Yaying Lou
Methodology: Jiangjie Yang, Zhijun Dai, Sergio Fagherazzi
Resources: Zhijun Dai, Yaying Lou
Software: Sergio Fagherazzi
Supervision: Zhijun Dai
Validation: Jiangjie Yang, Zhijun Dai, Xuefei Mei
Visualization: Zhijun Dai
Writing – original draft: Jiangjie Yang, Zhijun Dai

Abstract The Mississippi River Bird-foot Delta (MRBD) has long been at risk of deterioration due to Relative Sea Level Rise (RSLR), yet information on historical spatial distribution in wetland gain and loss remains limited. Using a Random Forest algorithm in Google Earth Engine, we extract wetland area from multiple Landsat images spanning 1990–2022. Data are integrated with sediment load, wave dynamics, sea level, and surface elevation to analyze drivers of wetland gain and loss. Results indicate a minor net change of only 1.21 km^2, with a total gain of 160.83 km^2 and a total loss of 159.62 km^2. Overall stability of wetland area masks significant regional variability, with notable wetland expansion in the interior and substantial losses along eastern and southeastern margins. Sediment diversion toward the interior of the delta lead to distributaries narrowing (Main Pass and Pass a Loutre) that further hindered sediment-laden water transport into deltaic margins. Wetland dynamics along the edges were closely linked to wave action, with large-scale retreat in northern (4.0 ± 9.9 m/yr), eastern (58.0 ± 48.2 m/yr), and southeastern (38.6 ± 15.8 m/yr) regions, while progradation in the southern (13.6 ± 10.1 m/yr) and western areas (7.4 ± 19.4 m/yr). Fluvial sediments significantly impact wetland growth with 1-year lag. Vertical accretion of wetlands exceeds RSLR, indicating equilibrium along vertical dimension but are affected by lateral dynamics driven by wave and fluvial sediment inputs. In conclusion, the MRBD is abandoning the distal parts to wave erosion, while focusing on building wetlands in the interior to create a more compact delta.

Plain Language Summary Sea level rise has attracted significant attention on the fate of the Mississippi River Bird-foot Delta (MRBD) in future years. In this study, we measured the gain and loss of MRBD and found that: (a) The land of MRBD did not experience uniform shoreline retreat and deltaic inundation despite rapid relative sea level rise. (b) The net gain of land in the MRBD was only 1.21 km^2 over the recent 32 years, with an actual land loss of about 159.62 km^2 and a land gain of about 160.83 km^2. (c) Fluvial sediments supply significantly impacted land growth of the MRBD with a 1-year lag. (d) Lateral erosion in the eastern and southeastern MRBD was caused by the persistent waves action from the east and south, and it was further exacerbated by narrowing of deltaic distributaries (Main Pass and Pass a Loutre), which directly hindered the transport of water and sediment into deltaic margins. The findings of this study can inform future restoration initiatives and contribute to the sustainable management of comparable deltaic wetland system across the world.

1. Introduction

Deltaic wetlands are vital coastal ecosystems that protect and sustain the livelihood of hundreds of millions of people worldwide (Beltrán-Burgos et al., 2023; Dunn et al., 2019; Overeem & Syvitski, 2009). Adequate sediment supply has been promoting the expansion of river deltas since their formation (Besset et al., 2019). In recent decades, widespread concern has arisen that a significant reduction in global sediment flux to the oceans, caused by damming and soil conservation efforts, could shift deltaic wetlands from progradation to retreat (Dunn & Minderhoud, 2022; Overeem & Syvitski, 2009). Rapid Relative Sea Level Rise (RSLR) has put deltaic wetlands at risk of drowning when vertical accretion rates are insufficient (Blum & Roberts, 2009; Nienhuis et al., 2023). Wave-driven erosion has also played a major role in deltaic wetland loss (Amer et al., 2017; Day et al., 2000; Howes et al., 2010).

Furthermore, deltaic wetlands have undergone complex changes influenced by both natural factors and human activities (Amer et al., 2017; Schuerch et al., 2018; Yang et al., 2021). For instance, the wetlands of the

Writing – review & editing:
Jiangjie Yang, Zhijun Dai, Sergio Fagherazzi

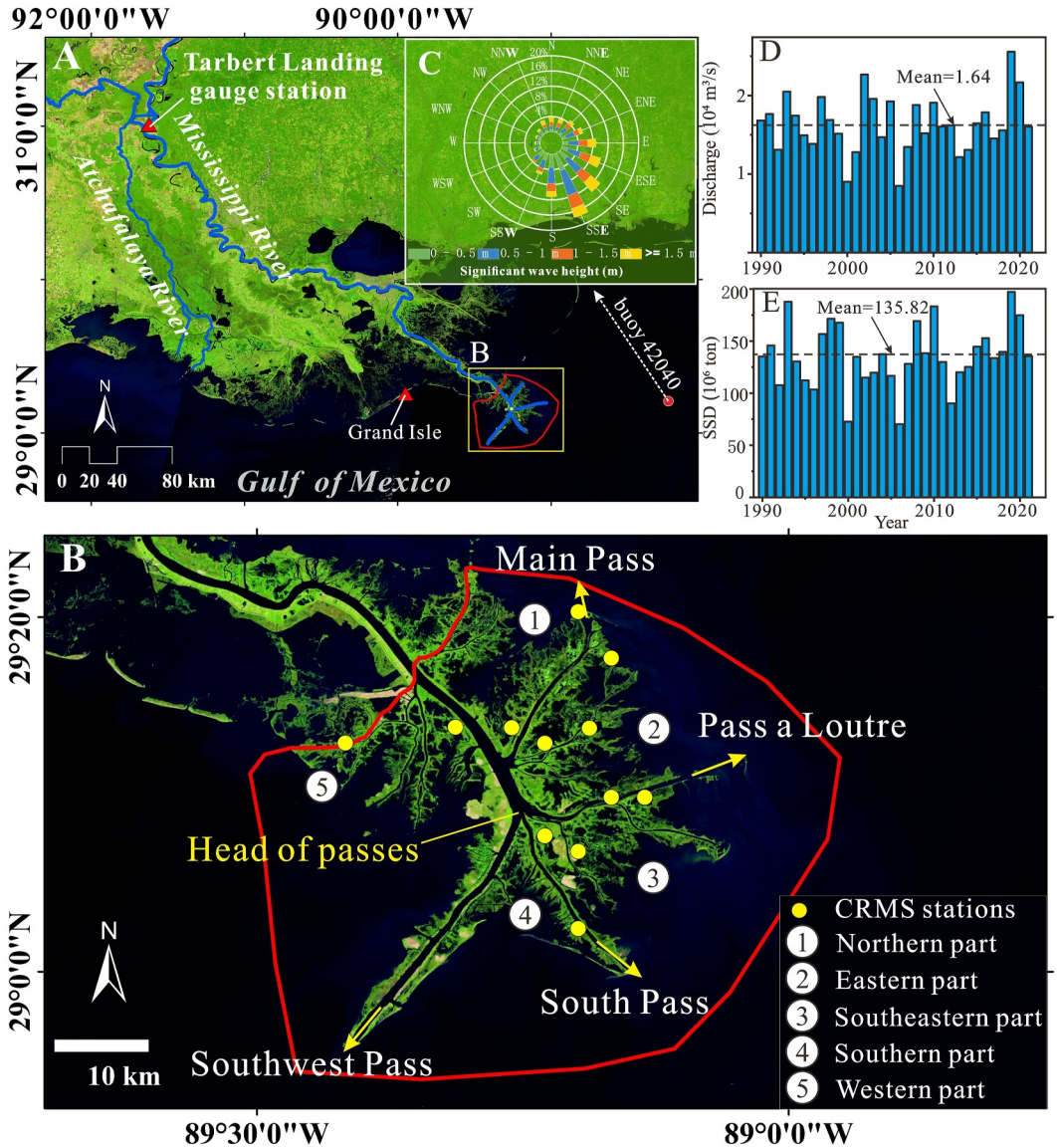

Figure 1. (a) Lower Mississippi River, Louisiana USA; (b) Mississippi River Bird-foot Delta; (c) Wave direction and significant wave height at buoy 42040; (d) Annual water discharge and (e) Suspended sediment discharge from 1990 to 2021.

Changjiang Estuary (Yangtze) Delta have gained about 916.90 km^2 from 1986 to 2018, despite a drastic decrease in sediment load since the construction of the Three Gorges Dam in 2003 (Chen et al., 2022; Dai et al., 2014, 2015). In contrast, more than 50% of the shoreline of the Mekong Delta experienced net erosion between 2003 and 2012, driven by reduced sediment supply from upstream dams, sand mining, levees, and channel modifications that disrupted its sediment balance (Anthony et al., 2015). Over the past century, approximately 4,877 km^2 (~25%) of coastal Louisiana's wetlands have been transformed into open water, making the Mississippi River Delta one of the most rapidly changing environments on Earth (Couvillion et al., 2011; Giosan et al., 2014; Syvitski & Saito, 2007).

The Mississippi River Bird-foot Delta (MRBD, Figures 1a and 1b), located at the modern mouth of the Mississippi River, has undergone significant wetland changes in the past century and it is now at risk of drowning (Blum & Roberts, 2009; Ericson et al., 2006; Nienhuis et al., 2020). Wetlands in the MRBD have lost approximately 370 km^2 between 1932 and 2016 (Couvillion et al., 2017). A massive reduction in sediment load has caused the deterioration of some lobes of the MRBD (Wells & Coleman, 1987) and human-altered sediment budgets have also generated significant wetland loss in the nearby Barataria Basin (Edmonds et al., 2023).

Overall, the fate of the Mississippi deltaic wetlands could be tied directly to vertical accretion (Chenevert & Edmonds, 2024). Blum and Roberts (2009) estimated that the MRBD will be submerged by the year 2100 owing to subsidence and SLR, in the absence of sediment inputs. To mitigate wetland loss, river diversion and dredging activities have been proposed effective restoration strategies (Allison et al., 2017; Amer et al., 2017). Additionally, autogenic process, such as avulsions and crevasse splays, play a crucial role in deltaic wetland resilience and long-term stability (Cahoon et al., 2011). A series of studies have demonstrated that during the formation and evolution of deltaic islands, there has been a shift from allogenic to autogenic processes controlling elevation over a 7-year period (Cahoon et al., 2011; Twilley et al., 2019; White, 1993).

Historic maps, navigation charts, and aerial photographs have been used in the past to analyze the evolution of the MRBD. These types of analyses are often time-consuming and the obtained data sets lack of temporal continuity (Wells & Coleman, 1987). Recently, an increasing number of researchers have utilized remote sensing images to analyze the spatiotemporal variations of the MRBD, due to the long-term, continuous, and easily accessible nature of the data (Amer et al., 2017; Couvillion et al., 2017). Couvillion et al. (2017) reported that more than 50% of the wetlands in the MRBD were lost from 1932 to 2016, based on a combination of historical data, aerial photography, and Landsat images. However, there is a limited amount of research on the spatial distribution of wetland gains and losses in the MRBD in the past 30 years. Therefore, combining remote sensing images, hydrological data (including fluvial sediment load, wave and sea level data), along with surface elevation data from 1990 to 2022, here we aim to: (a) determine what parts of the MRBD are prograding or receding; (b) detect whether variability in sediment supply is related to wetland gain or loss in the MRBD; (c) identify whether MRBD is drowning due to RSLR; (d) determine whether other drivers are responsible for wetland gain and loss in the MRBD. The findings of this study will offer critical insights into the spatial gains and losses of MRBD wetlands and have significant implications for the survival of deltas in the context of rapid sea level rise and extensive human interference.

2. Material and Methods

2.1. Study Area

The MRBD is a micro-tidal, river-dominated delta, and its growth is dominated by fluvial processes and influenced by RSLR (Blum & Roberts, 2009; Olson & Suski, 2021). The MRBD wetlands are minimally affected by daily tides, as the mean tidal range is only about 32 cm, resulting in limited tidal-driven transport of water and sediment (Day et al., 2007; Hiatt et al., 2019). The delta is characterized by vegetation zonation—comprising salt, brackish, intermediate, and freshwater marshes—primarily determined by salinity gradients (Day et al., 2000; Figure S1c in Supporting Information S1). Four main distributary channels (Main Pass, Pass a Loutre, South Pass, and Southwest Pass) divide the MRBD in five components: the northern, eastern, southeastern, southern, and western parts (Figure 1b). These regions exhibited different hydrodynamic characteristics, including variations in riverine discharge, sediment supply, and wave exposure.

2.2. Data Collection

Remote sensing images from 1990 to 2022 with cloud cover of less than 30% were obtained from Google Earth Engine (GEE, https://code.earthengine.google.com/), including Landsat-5 TM (1990–2011), Landsat 8 OLI (2013–2019), and Sentinel 2 (2020–2022). To minimize the impact of tidal levels and seasons on the delta evolution analysis, we have only selected images taken in winter or in the following early spring and with a tidal level ranging from −0.43 to 0.10 m (Table S1 in Supporting Information S1). Water discharge and Suspended Sediment Discharge (SSD) from 1990 to 2021 were collected at Tarbert Landing gauging station from the United States Geological Survey (USGS). Hourly wave direction angle and significant wave height at buoy 42040 (88° 14′12″W, 29°12′24″N), located about 98 km east of the Head of Passes, were downloaded from the National Oceanic and Atmospheric Administration (NOAA) for 1996–2022. Tidal levels and sea level data at Grand Isle from 1990 to 2023 were derived from NOAA. Marsh surface elevation data from 2007 to 2022 were measured with Rod Surface Elevation Tables by the Coastwide Reference Monitoring System (CRMS) with a vertical precision of ∼1.0–1.5 mm (Cahoon et al., 2002, 2020). Vegetation type for 1997, 2001, 2007, 2013, and 2021 were derived by CRMS with field survey. Coastal vegetation data with a spatial resolution of 30 m (2017 Coastal Master Plans) was downloaded from the Coastal Protection and Restoration Authority (CPRA) (Figure S1 in

Supporting Information S1). Furthermore, the Coastal Digital Elevation Model (DEM) of Southern Louisiana was downloaded from NOAA with a spatial resolution of 10 m.

2.3. Image Processing

Remote sensing images taken in winter or in the following early spring were selected each year as representative of the delta extension for the current year. A Random Forest algorithm based on GEE was utilized to classify available satellite images into water and emergent deltaic wetlands (Amer et al., 2017; Beltrán-Burgos et al., 2023). The algorithm was used to assess gains and losses of the MRBD from 1990 to 2022. All processing was performed after removing clouds and cloud shadows. We first selected hundreds of deltaic wetland and water polygons for each image by visual interpretation. We then selected 1500 sample points using the "random Point" command in GEE to generate deltaic wetland and water body layers (Figure S1a in Supporting Information S1). Five bands and three spectral indices extracted from remote sensing images were employed as input variables for the Random Forest classifier (Table S2 in Supporting Information S1) to classify the images into deltaic wetland and water. Finally, a confusion matrix and evaluation metrics (overall accuracy and kappa coefficient) were used for validation and accuracy assessment. The validation data for each year was created based on the vegetation data downloaded from CRMS combined with historical images from Google Earth (Figure S1b in Supporting Information S1). Both overall accuracy and kappa coefficient were greater than 85% for each year in the classification process, meeting the requirement for accurate classification (Table S1 in Supporting Information S1) (Kumar et al., 2021). Furthermore, we selected imagery in winter-early spring, to avoid the growing season and reduce the effect of submerged and floating vegetation. We found that the area of floating vegetation in 2017 was less than 1% of the MRBD area (Figure S1c in Supporting Information S1), and therefore considered the influence of submerged and floating vegetation on our classification results small enough to be negligible.

Visual interpretation was utilized to distinguish new wetlands created by dredged soil, which appeared suddenly with clear boundaries and white or pink pixels on Landsat images (Zhang et al., 2021) (Figure S2 in Supporting Information S1). These landforms, distinctly different from the surrounding vegetation, were outlined manually and their area computed in ArcGIS.

2.4. Digital Shoreline Analysis System (DSAS)

DSAS is a computer software extension of ArcGIS, providing a method for the calculation of historical shoreline change (https://code.usgs.gov/cch/dsas). This software can calculate a range of statistical variables based on shorelines extracted in different years, including NET Shoreline Movement, Shoreline Change Envelope, End Point Rate (EPR), and Linear Regression Rate. EPR is the rate at which the shoreline has moved during the time elapsed between the oldest and most recent measurements. In this study, the shoreline was defined as the interface between wetland and water, which is similar to the hydrodynamic shoreline of Geleynse et al. (2015). The shoreline was derived from the results of the GEE classification and manually outlined to ensure accuracy and continuity. Subsequently, we used DSAS to calculate shoreline change at each 4–5-year interval from 1990 to 2022 along 585 transects spaced 300 m (Figure 2c). The envelope area (A_e) between two shorelines reflect the effect of waves and sediment deposition on deltaic wetland. EPR and A_e are defined as follows:

$$\mathrm{EPR} = \frac{\Delta D}{\Delta Y} \tag{1}$$

$$A_e = \sum_{1}^{585} \mathrm{EPR} * d * \Delta Y \tag{2}$$

where ΔD is the distance in meters between two shorelines; ΔY is the time elapsed between the oldest and most recent measurements; and d is the distance between two transects.

In order to analyze the width variations of the distributary channels, the channel banks along the four main branches were artificially outlined according to the classification results. We then created a series of transects at 1 km interval from the head to the terminal end of each pass, and used them to systematically measure channel width at each interval. The channel width is calculated as the distance between the two banks along each transect, and it was taken approximately every 4–5 years to capture time variations (Figure S3 in Supporting Information S1).

10.1029/2024EF005003

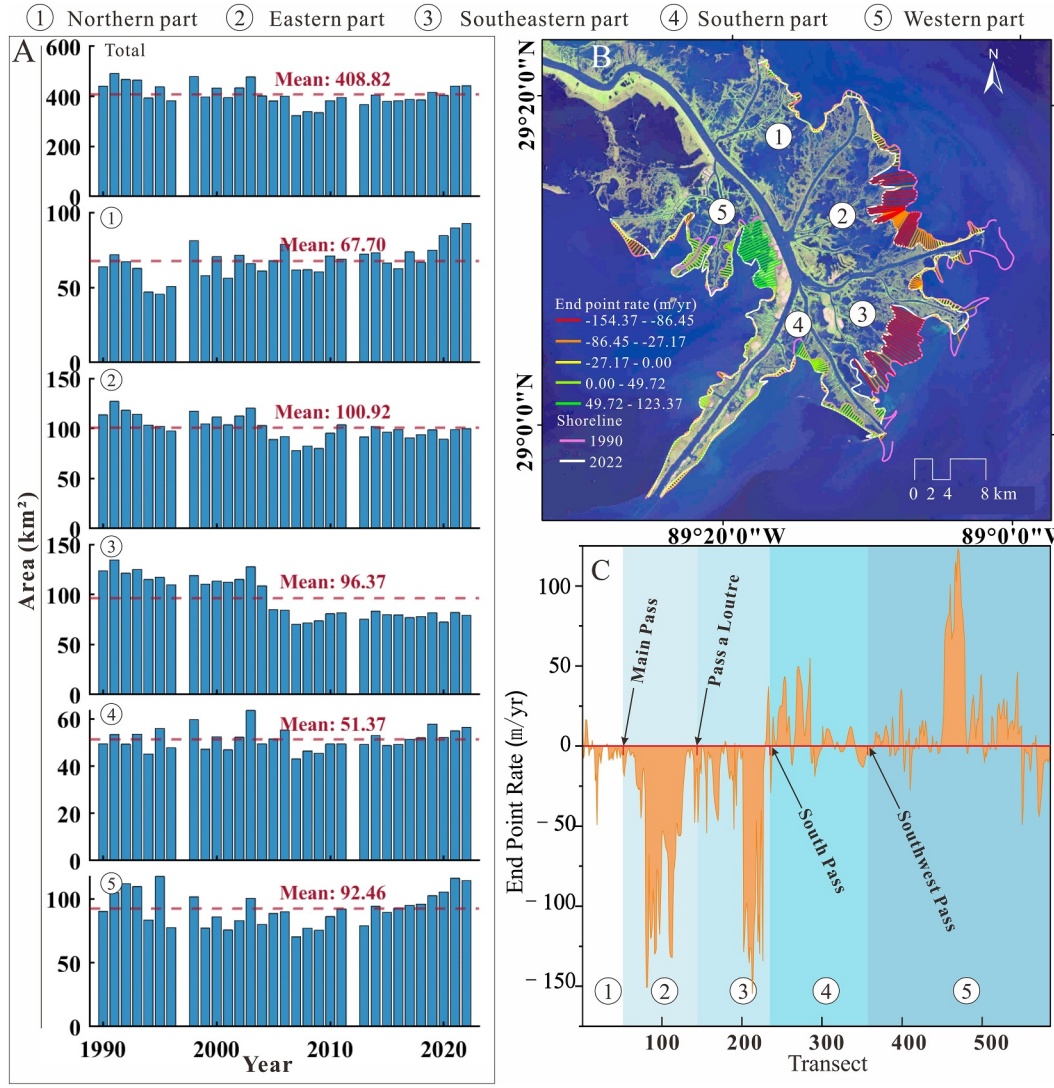

Figure 2. Wetland area and shoreline change in the Mississippi River Bird-foot Delta. (a) Long-term wetland area changes in different parts of the delta; (b) Shorelines and transects; (c) End point rate of transects. End point rate is the rate at which the shoreline moved during the time elapsed between the oldest and most recent measurements.

2.5. Wave Energy Calculation

We categorized the wave measurements into 16 directions based on their incidence angle, each spaced by 22.5° (Table S3 in Supporting Information S1). We subsequently analyzed the wave data by wave height. A grouped frequency distribution was used by dividing wave amplitudes in multiple class intervals based and calculating relative frequency and relative cumulative frequency for each interval (Mei et al., 2015). The mean wave energy (E, J/m^2) was calculated per unit of horizontal area as follows (Battjes & Janssen, 1978; Table S3 in Supporting Information S1):

$$E = \frac{1}{16}\rho g H^2 \tag{3}$$

where: ρ is the density of seawater (kg/m^3), g is gravitational acceleration (9.8 m/s^2), and h is the significant wave height (m). The sum of the mean wave energy for each direction is the cumulative wave energy.

2.6. Surface Elevation Measurements

Changes in surface elevation were estimated by CRMS using the Rod Surface Elevation Table method. At every CRMS site, a designated Rod Surface Elevation Table benchmark was installed from which the surface elevation was measured at nine points across four directions. These measurements were repeated every 6-month to calculate elevation change. The mean cumulative elevation change is computed for each sampling site along four directions and elevation change rate is estimated by using linear regression of elevation change against time.

2.7. Sensitivity of Wetland Area and Shoreline Location With Respect to Water Levels

Variations in water levels across different Landsat images can lead to errors in the analysis of shoreline position and wetland area (Figure S4 in Supporting Information S1). The slope of each transect is calculated as follows:

$$\text{Slope} = \frac{\Delta H}{D} \tag{4}$$

where: ΔH (m) is the elevation difference between the start and end of the transect extracted from the DEM, and D (m) is the length of the transect. Negative slope values were eliminated and the average slope of the remaining transects was calculated. This slope was assumed to be the representative slope of the distal MRBD. The horizontal displacement (s, m) of the shoreline along each transect caused by water level differences across images is calculated as follows:

$$s = \frac{\Delta h}{\text{Slope}} \tag{5}$$

where: Δh (m) is the difference in water level between two remote sensing images and Slope is the average slope. The mean distance of shoreline movement at each 4–5 years interval is the average of the distances along the shoreline in the transect direction (Table S4 in Supporting Information S1). The area (A, km^2) affected by the water level difference is calculated as follows:

$$A = \sum s * d \tag{6}$$

where: d is the distance between two transects, that is, 300 m. Errors in wetland area and shoreline movement can be expressed as percentage of the average wetland area and mean shoreline movement distance obtained from remote sensing (Table S4 in Supporting Information S1).

3. Results

3.1. Areal Change of the MRBD

Between 1990 and 2022, the wetland area of MRBD fluctuated between 323.01 and 478.76 km^2, with an average area of 408.82 km^2. Specifically, the wetland area initially increased, peaking at 478.76 km^2 in 1998, then decreased to a minimum of 323.01 km^2 by 2009, before beginning to increase again. Despite these fluctuations, the wetland area remained relatively stable in the first and last years of the study period, with values of 440.97 km^2 in 1990 and 442.54 km^2 in 2022 (Figure 2a).

From a regional perspective, the wetland areas across the five zones showed distinct trends, reflecting spatial heterogeneity in the deltaic evolution. The northern part increased from 63.72 km^2 in 1990 to 92.61 km^2 in 2022. In contrast, both the eastern and southeastern parts displayed a decreasing trend, with net losses of 13.91 and 44.43 km^2, respectively. Meanwhile, the southern and western parts did not display significant trend, fluctuating around 51.37 and 92.46 km^2, respectively (Figure 2a).

3.2. Gain and Loss in the MRBD

The distribution of wetland gain and loss in the MRBD over the past 32 years is shown in Figure 3a (see also Figure S5 and Table S5 in Supporting Information S1). Between 1990 and 2022, the wetland area of total MRBD experienced a net gain of only 1.21 km^2, with a loss of about 159.62 km^2 and a gain of about 160.83 km^2

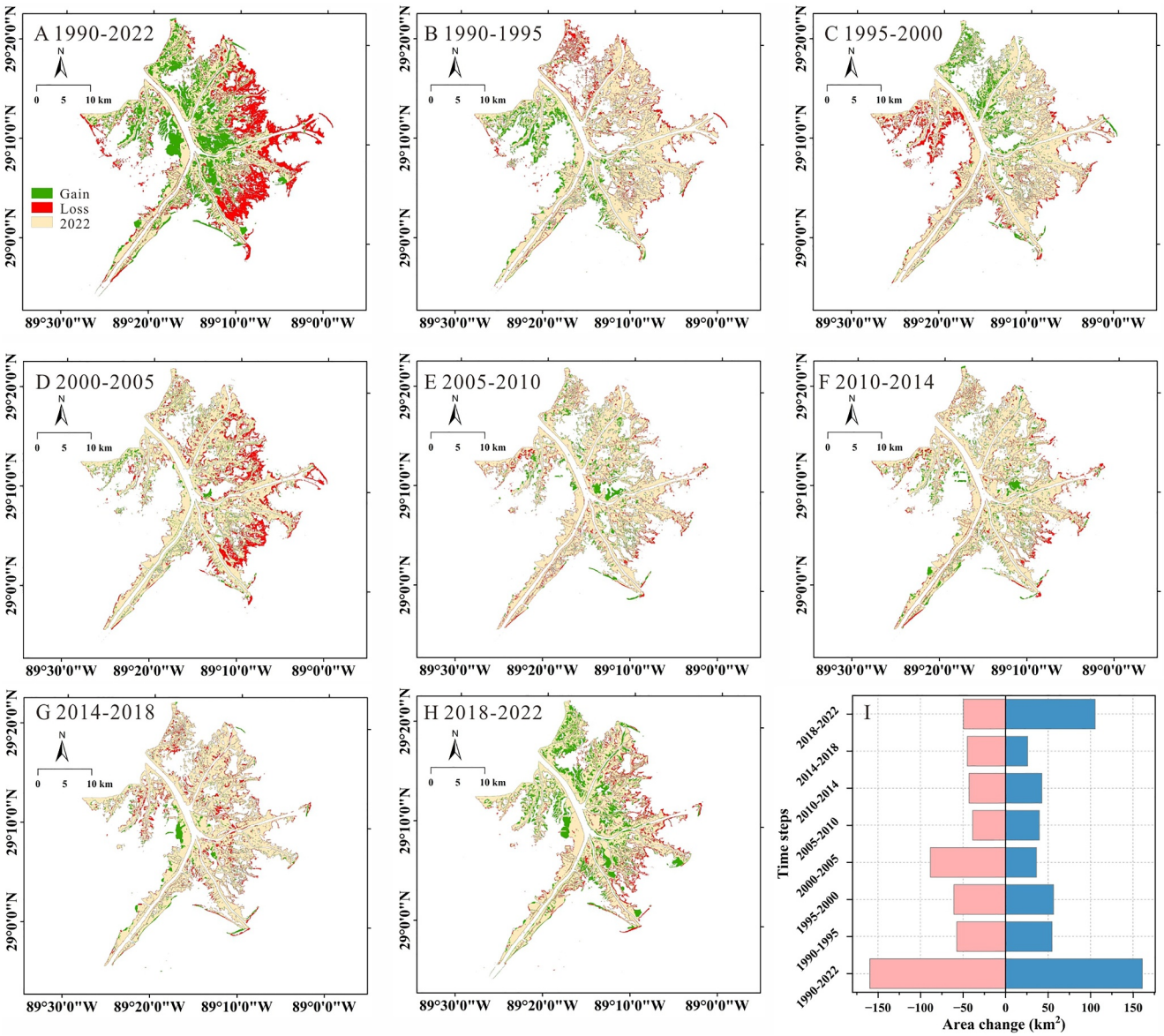

Figure 3. Gain and loss of Mississippi River Bird-foot Delta wetlands over 4–5 years intervals. (a–h) Spatial land gain and loss; (i) Temporal land gain and loss.

(Figures 3a and 3i). Wetland deterioration primary occurred along the eastern and southeastern margins, where shoreline retreat resulted in losses of approximately 52.51 and 69.14 km^2, respectively. These losses accounted for about 11.9% and 15.7% of the wetland area in 1990, and equivalent to approximately 32.9% and 43.3% of the total wetland loss. In contrast, notably wetland expansion occurred in the interior of the MRBD, particular in the riverside sections of the northern, eastern, and western parts, where filling of internal bays resulted in gains of 37.04, 38.61, and 43.17 km^2. These gains represent about 8.4%, 8.8%, and 9.8% of the wetland area in 1990, corresponding to approximately 23.0%, 24.0% and 26.8% of the total wetland gain (Figure 3a).

Moreover, we analyzed the spatial distribution of wetland changes at 4-5-year intervals and observed wetland degradation at the distal end of the delta, along with internal expansion (Figures 3b–3h). From 1990 to 2014, the net wetland area exhibited minimal change, with gains and losses largely balancing each other during this period (Figures 3b–3f). The most significant wetland loss occurred between 2000 and 2005, with approximately 88.38 km^2 lost, mainly along the eastern and southeastern margins (Figure 3d). The notable wetland gain was observed between 2018 and 2022, with the northern and western regions experiencing the creation of approximately 105.36 km^2 of new wetland (Figure 3h).

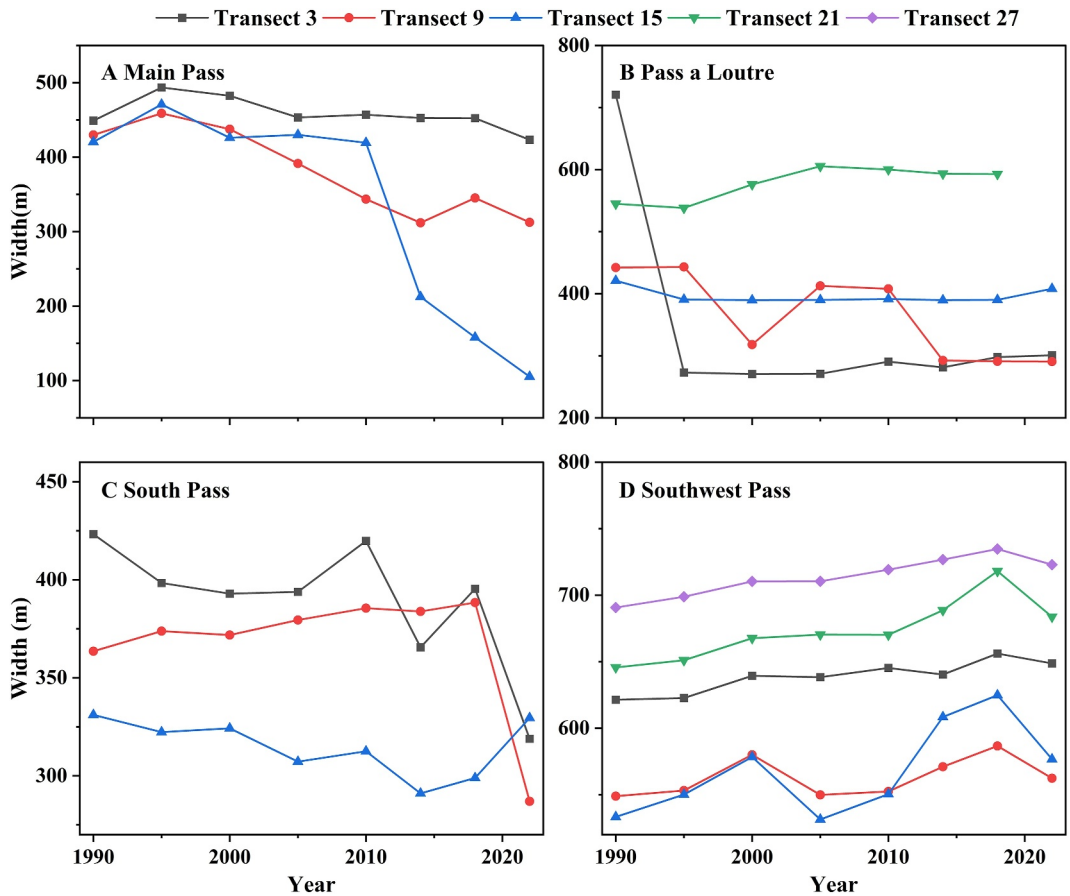

Figure 4. Width variations of the four main distributaries.

3.3. Change in Shorelines and Distributaries of the MRBD

Our analysis shows that shoreline changes in the MRBD were spatially heterogeneous over the past 32 years, with retreated along the northern, eastern, and southeastern shorelines, while the southern and western shorelines advanced seaward (Figures 2b and 2c). On average, the eastern shoreline experienced the most significant retreat at 52.0 ± 48.2 m/yr, followed by the southeastern shoreline at 38.6 ± 15.8 m/yr, indicating notable erosion in both regions. In contrast, the northern shoreline receded at a much slower rate of 4.0 ± 9.9 m/yr, with greater variability suggesting localized erosion and deposition processes (Figures 2b and 2c). The southern and western shorelines showed progradation, with the western shoreline advancing at a relatively stable rate (7.4 ± 19.4 m/yr) compared to the more variable progradation observed along the southern shoreline (13.6 ± 10.1 m/yr) (Figures 2b and 2c). The wetland area enclosed between the 1990 and 2022 shorelines experienced a net loss of 43.3 km^2 (93.6 km^2 lost and 50.3 km^2 gained). Overall, these wetland gains between the two shorelines offset approximately 31.5% of the total wetland loss recorded across the MRBD between 1990 and 2022.

These shoreline changes were accompanied by notable variations in the width of the four main distributaries from 1990 to 2022 (Figure 4). Specifically, the Southwest Pass exhibited a slight widening trend (Figure 4d). In contrast, the other three passes exhibit varying degrees of narrowing, with the most pronounced narrowing occurring in Main Pass (Figure 4a), followed by Pass a Loutre (Figure 4b), and then South Pass (Figure 4c). These narrowing trends were primarily characterized by the formation of numerous new sandbars, with an area of 2.0 km^2, 2.5 km^2, and 0.8 km^2, respectively (Figure S3 in Supporting Information S1).

4. Discussion

4.1. Impact of Riverine Sediment Supply

Fluvial sediment is the primary source of material in river-dominated deltas, and the amount of sediment deposited on the delta topset controls deltaic wetland gain and loss (Dai, 2021; Edmonds et al., 2023; Nardin & Edmonds, 2014; Nardin et al., 2016; Olson & Suski, 2021). A reduction in riverine sediment supply caused by human activities (including damming and levee construction) can jeopardize fluvial deltas, since deltaic regions require adequate sediment supply and deposition to counteract subsidence and SLR (Blum & Roberts, 2009; Edmonds et al., 2023; Ericson et al., 2006). From 1990 to 2021, the annual average SSD and water discharge of the lower Mississippi River were 135.82×10^6 ton and 1.64×10^4 m^3/s, with no significant long-term variations (Figures 1d and 1e). Herein, the positive correlation between SSD and net wetland area variations indicates that the river sediment load plays a crucial role in controlling the overall expansion of the delta (Figures 5a and 5b). However, this correlation exhibits a lagged effect, where the sediment load of the current year influences the wetland area change of the following year (Figure S6 in Supporting Information S1). The lack of correlation between SSD and variations in wetland area in each part of the delta implies that local growth is not controlled by fluvial load only (Figures 5c–5f), but is subject to other external factors that alter the role of riverine sediment. The effects of other external drivers will be discussed in subsequent sections.

4.2. Impact of Relative Sea Level Rise

The MRBD is widely recognized as being highly vulnerable to submergence due to RSLR (Blum et al., 2023; Fagherazzi et al., 2020), which averaged 22.08 mm/yr from 1990 to 2022. This rate includes a sea-level rise rate of 8.6 mm/yr at Grand Isle (Figure S7b in Supporting Information S1), and a total subsidence rate of 13.48 mm/yr (Jankowski et al., 2017). Despite the high rate of RSLR, there is little evidence of widespread submergence across the entire MRBD, as indicated by contrasting shoreline dynamics: while the northern, eastern, and southeastern shorelines retreated, the southwestern and western shorelines advanced (Figures 2b and 2c). Furthermore, the average vertical accretion rate across multiple monitoring stations within the deltaic wetlands was 32.4 ± 12.6 mm/yr (Figures S7 and S8 in Supporting Information S1), which also accounts for shallow subsidence of 7.77 mm/yr (Jankowski et al., 2017). Since this accretion rate exceeds the RSLR rate of 22.08 mm/yr, RSLR did not pose an immediate risk of drowning to the MRBD during the study period. Nevertheless, it is important to note the presence of eroding shorelines within the area, indicating that while the system is stable in the vertical direction, it is undergoing changes in the horizontal direction.

Furthermore, RSLR raises base levels in deltaic systems, increasing backwater effects and elevating upstream river water levels (Cox et al., 2022). This process reduces flow velocity within distributary channels and promotes in-channel sedimentation. Meanwhile, higher water levels also increase the likelihood of levee overtopping, thereby facilitating the formation of crevasse splays and localized avulsions (Chadwick et al., 2022). The implications of these processes for wetland changes in the MRBD are further discussed in Section 4.5.

4.3. Impact of Waves

Wave-driven erosion plays a significant role in the deltaic wetland loss, particularly in regions exposed to high wave energy (Anthony et al., 2015; Day et al., 2000). In the Mississippi Delta, waves are responsible for approximately 26% of wetland loss (Penland et al., 2000), primarily by causing edge erosion (Day et al., 2023). Consistent with these findings, significant wetland retreat has been observed along the eastern and southeastern margins of the MRBD, with losses of approximately 45.9 and 34.8 km^2, respectively (Figures 2b and 3a). This retreat corresponds to high wave energy ($\sim 8.2 \times 10^7$ J/m^2), predominantly caused by waves propagating from the east and the south (Table S3 and Figure S9 in Supporting Information S1). The direct impact of waves triggers erosion and wetland degradation, exacerbating the vulnerability of exposed shorelines. In contrast, the western MRBD experiences reduced wave impact due to the shielding effect ok wetlands in West Bay, which helps minimize shoreline erosion in this region (Figures 2b and 3a). The stark contrast in wave exposure between the eastern/southeastern and the western shorelines highlights the critical role of wave energy in driving wetland dynamics and delta stability. Overall, wave-driven erosion has significantly contributed to wetland loss in the eastern and southern MRBD.

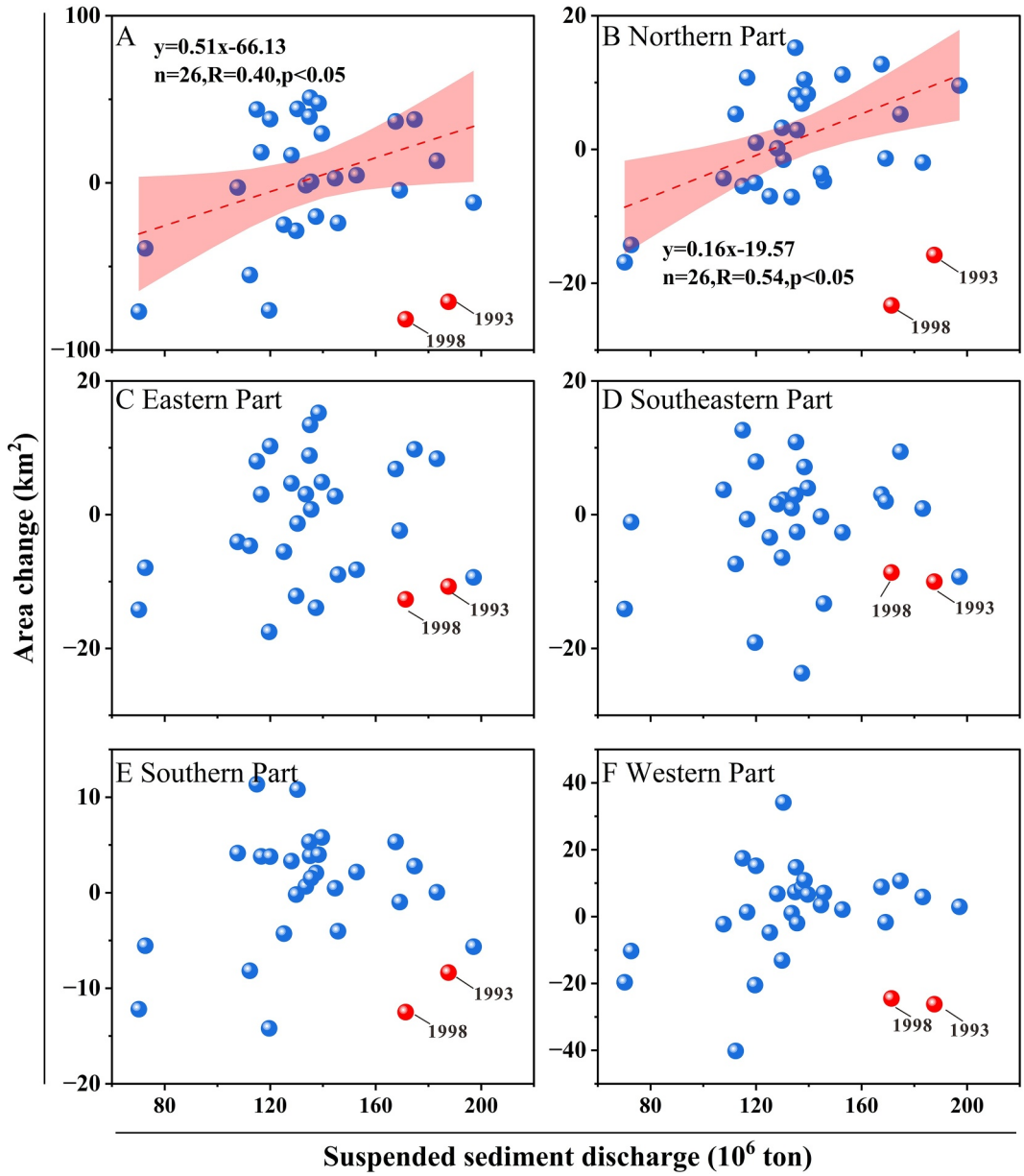

Figure 5. Correlation between wetland area change in each part of the Mississippi River Bird-foot Delta and Suspended Sediment Discharge (SSD). The wetland area change is the difference between the wetland area of the following year minus the wetland area of the current year. The SSD is the average value of the current year. High water discharge with high SSD occurred in both 1993 and 1998.

4.4. Impact of Autogenic Processes

Autogenic processes have significantly impacted the dynamic evolution of deltaic wetlands in the Mississippi delta. Over centennial timescales, delta lobe switching has determined the long-term shift of depositional centers, leading to the gradual abandonment of older deltaic regions and the redirection of sediment supply toward newly active areas (Jerolmack, 2009; Paola, 2016). Similar processes occur in the MRBD, where crevasse splays and localized avulsions play a crucial role in wetland formation and maintenance processes decadal timescales (Cahoon et al., 2011). When floodwaters breach levees and deposit sediment into interior deltaic bays, crevasse splay contributes to localized land building and wetland expansion (Coleman, 1988). Initially, sediment infilling leads to the emergence of mud surfaces, creating suitable conditions for vegetation colonization (Cahoon et al., 2011). Once established, vegetation stabilizes the sediment, reduces flow velocity, and enhances sediment

trapping, promoting further accretion and land elevation (Fagherazzi, 2008; Hou et al., 2024). This vegetation-sediment feedback fosters wetland persistence by reinforcing surface stability and sustaining long-term vertical growth. Remote sensing observations indicate that fragmented vegetation patches have progressively coalesced into larger, contiguous wetlands (Figures S10b and S10c in Supporting Information S1), which has facilitated vegetation expansion within the delta interior (Figure 3a), further enhancing delta stability.

Furthermore, distributary channel narrowing has played a significant role in wetland redistribution. Combined with backwater effect and velocity reduction caused by RSLR, sediment accumulates within active channels (Main Pass, Pass a Loutre, and South Pass), promoting the formation of sandbars and constricts channel width (Figure 4; Figure S3 in Supporting Information S1). Research by Cook et al. (2020) and Whitbread et al. (2015) indicates that the width of distributary channels scales with discharge and therefore controls sediment load. While sandbars formation locally increases wetland area, it also reduces sediment transport to distal deltaic regions, exacerbating wetland loss along the edges of the northern, eastern, and southeastern MRBD. This redistribution of sediment, combined with wave energy, intensifies spatial heterogeneity in wetland change. In areas exposed to strong hydrodynamic forces, sediment deficits accelerate wetland loss, while more sheltered regions experience continued expansion. This interaction between autogenic processes and external forcings leads to the complex and heterogeneous patterns of wetland gain and loss observed in the MRBD. Overall, these autogenic dynamics have played a critical role in shaping the MRBD wetlands, particularly by fostering localized expansion in sediment-rich zones while indirectly contributing to wetland retreat in sediment-deficient areas.

4.5. Impact of Anthropogenic Activities

The diversion of sediment-laden water from distributaries to adjacent wetlands can mitigate wetland loss (Allison et al., 2017). The West Bay Diversion completed in November 2003 transports freshwater and sediment from the main stem of the Mississippi River to the West Bay, facilitating wetlands expansion (Allison et al., 2017; Figures S11a and S11b in Supporting Information S1). Deposition of dredged soil is beneficial for the creation and restoration of degraded vegetated wetlands in shallow open waters (Amer et al., 2017). Between 2009 and 2014, federal and local authorities built oblong islands in West Bay using pipe-lined soil from dredging of the adjacent navigation channels. These islands are intended to increase sediment trapping efficiency by reducing water velocity and limiting wave fetch (Allison et al., 2017; Figures S11g and S11h in Supporting Information S1). Through visual interpretation, we found that deposition of dredge sediment led to a local wetland gain of 14.0 km^2 in the interior of the eastern and southeastern parts, as well as in West Bay. This gain compensated 8.7% of the total wetland loss between 1990 and 2022 (Figures S11c–S11l in Supporting Information S1).

4.6. Conceptual Model of MRBD Evolution

Together, the data analysis presented herein can be combined in the following conceptual model of the evolution of the MRBD (Figure 6): (a) Riverine sediment fluxes drive the expansion and contraction of the delta with a lag time of approximately 1 year. (b) Autogenic processes—including crevasse splay formation, localized avulsions, and vegetation colonization—redirect sediment to the delta interior, promoting deposition and interior wetland growth, while leading to silting of distributaries and reduced sediment delivery to distal wetlands. (c) Narrowing channels caused by new sandbars hinder sediment delivered to distal areas. (d) Relative sea level rise enhances backwater effect and reduces flow velocity within distributary channels, exacerbating sedimentation in channel and further diverting sediment away from distal areas. (e) The distal areas of the system are increasingly subject to erosion by wave action and reduced sediment inputs. (f) Diversion of sediment is exacerbated by dredging activities, which deposit material in the interior delta. (g) Increased sediment availability in the interior allows wetlands to vertically accrete and keep pace with sea level rise but also drives lateral reconfiguration of the delta. (h) The combination of these processes results in a more compact and uniform delta, reducing the extent of the bird's foot distributaries and related distal wetlands.

4.7. Uncertainty Analysis

The annual changes in deltaic wetland area exceed the size of a single pixel, confirming that changes are detectable at the pixel level. However, since this study employed a Random Forest classification approach, it did not account for sub-pixel variability. This could lead to overestimation or underestimation errors, especially at short timescales when only a few pixels shift between water and land. The classification's high overall accuracy

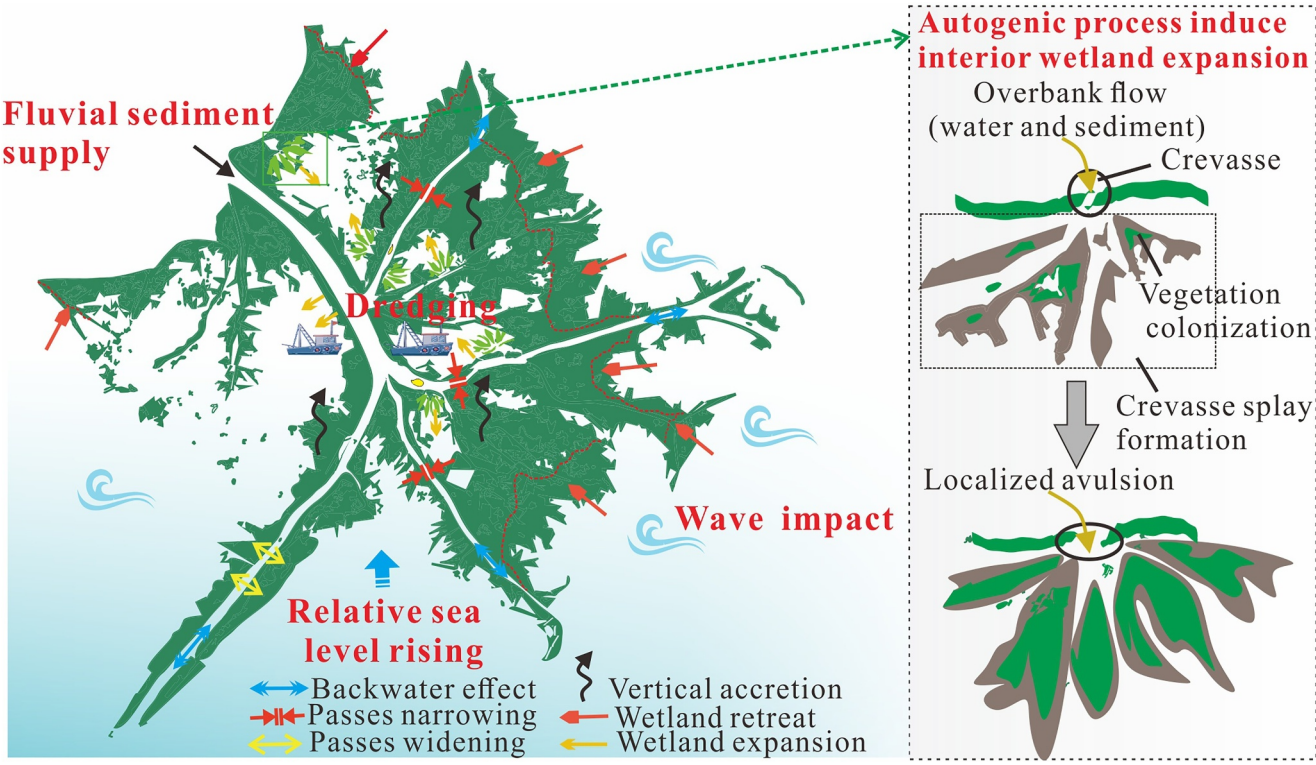

Figure 6. Conceptual model of wetland evolution in the Mississippi River Bird-foot Delta.

(more than 85%) and kappa coefficient means that our results are reliable (Table S1 in Supporting Information S1), as confirmed by previous studies (Aronoff, 1985; Congalton, 1991).

Furthermore, variations in water levels across the selected images from year to year could introduce errors in estimating the wetland change area. To address this, we used the equations in Section 2.7 to calculate the potential error in wetland area triggered by water level differences. Our results indicate that the area impacted by the maximum water level difference (0.45 m in the period of 2006–2007) is approximately 17.19 km^2, accounting for 4.17% of the annual average change in wetland area, suggesting that the influence of water level variations is relatively weak. Furthermore, the average horizontal displacement of the shoreline over a 4/5-year interval ranges from 121 to 214 m (Table S4 in Supporting Information S1), while the shoreline changes caused by a variation in water level of 0.05 m is 14.96 m. Consequently, the errors due to water level differences on shoreline distance during the periods 1990–1995, 1995–2000, 2000–2005, 2005–2010, 2010–2014, 2014–2018, and 2018–2022 were 153 m ± 17.33%, 144 m ± 10.15%, 174 m ± 3.67%, 210 m ± 15.23%, 155 m ± 8.83%, 214 m ± 6.81%, and 121 m ± 10.74%, respectively (Table S4 in Supporting Information S1). The errors associated with water levels on shoreline position and area estimation are thus within acceptable limits.

5. Conclusions

The wetlands of the MRBD have been a focal point for research and conservation projects due to their significant ecological, economic, and cultural importance. Local governments and organizations have invested substantial funds and efforts to protect these vital ecosystems. Our study leverages machine-learning methods to interpret remote sensing imagery, analyzing the wetland gains and losses in the MRBD. The main conclusions are as follows:

1. Between 1990 and 2022, wetlands area of the MRBD has experienced a dynamic equilibrium, with wetland gain of 160.83 km^2 and loss of 159.62 km^2. Spatial variations show a significant loss in the eastern and southeastern margins, while a notable expansion is present in the interior of the MRBD. Shoreline dynamics varied, with retreat in the northern (4.0 ± 9.9 m/yr), eastern (52.0 ± 48.2), and southeastern (38.6 ± 15.8 m/yr) parts, and progradation in the southern (7.4 ± 19.4 m/yr) and western (13.6 ± 10.1 m/yr) areas. Meanwhile,

several distributaries exhibited varying degrees of narrowing, as sand bars of 2.0 km^2, 2.5 km^2, and 0.8 km^2 emerged in the Main Pass, Pass a Loutre, and South Pass, respectively.

2. Fluvial sediment load has a significant impact on wetlands growth, with a lagged effect where current-year sediment inputs impacts next-year changes in wetland area. Relative sea level rise made minor contribution to the gain and loss of wetland in MRBD, as the vertical accretion rates (32.4 m ± 12.6 m) exceeds the rate of relative sea level rise (22.08 mm/yr). Long-term wave action was considered as the main driver of wetland loss in the eastern and southern margins.
3. Autogenic processes, such as crevasse splays and vegetation-sediment feedback, have contributed to wetland expansion in the interior of the MRBD. Narrowing of active channels (Main Pass, Pass a Loutre, and South Pass) has hindered the transport of fluvial water and sediment into seaward margins, intensified wetland loss and deterioration in distal regions. Human activities, including the West Bay Diversion and dredging projects, helped mitigate wetland loss by creating about 14.0 km^2 of new wetlands.

Data Availability Statement

Remote sensing images integrated from https://code.earthengine.google.com/ (Google, 2024), including Landsat 5 data from https://developers.google.com/earth-engine/datasets/catalog/LANDSAT_LT05_C02_T1_L2 (USGS, 2011), and Landsat 8 data from https://developers.google.com/earth-engine/datasets/catalog/LANDSAT_LC08_C02_T1_L2 (USGS, 2019), and Sentinel-2 data from https://developers.google.com/earth-engine/datasets/catalog/COPERNICUS_S2 (ESA, 2022) were used in the creation of this manuscript. Water discharge and suspended sediment discharge at Tarbert Landing gauge station were available through https://waterdata.usgs.gov/nwis/inventory?agency_code=USGS&site_no=07295100 (USGS, 2021). Hourly wave data at buoy 42040 from https://www.ndbc.noaa.gov/station_history.php?station=42040 (NOAA, 2021) and tidal levels data at Grand Isle from https://tidesandcurrents.noaa.gov/waterlevels.html?id=8761724 (NOAA, 2022) are downloaded from the NOAA website. To analyze the changes in surface elevation and vegetation distribution, marsh surface elevation data at 12 stations from 2007 to 2022 were collected from https://cims.coastal.louisiana.gov/masterplan/GISDownload/ (CRMS, 2022) and coastal vegetation data from https://www.lacoast.gov/crms_viewer/Map/CRMSViewer (CPRA, 2017) were collected. Local surveys of vegetation type in 1997 (Chabreck & Linscombe, 1997), 2001 (Linscombe & Chabreck, 2006), 2007 (Sasser et al., 2008), 2013 (Sasser et al., 2014), and 2021 (Nyman et al., 2022) were used to be validation data. The calculations of slope in the MRBD were based on Coastal Digital Elevation Model of Southern Louisiana from https://www.ncei.noaa.gov/access/metadata/landing-page/bin/iso?id=gov.noaa.ngdc.mgg.dem:1521 (NOAA, 2015).

Acknowledgments
This study was supported by National Key R&D Program of China (2023YFE0121200), the National Natural Science Key Foundation of China (42430406), and Shanghai International Science and Technology Cooperation Fund Project (23230713800). Sergio Fagherazzi was partly funded by the USA National Science Foundation Award 2224608 (PIE LTER) and 1832221 (VCR LTER).

References

Allison, M. A., Yuill, B. T., Meselhe, E. A., Marsh, J. K., Kolker, A. S., & Ameen, A. D. (2017). Observational and numerical particle tracking to examine sediment dynamics in a Mississippi river delta diversion. *Estuarine, Coastal and Shelf Science*, *194*, 97–108. https://doi.org/10.1016/j.ecss.2017.06.004

Amer, R., Kolker, A. S., & Muscietta, A. (2017). Propensity for erosion and deposition in a deltaic wetland complex: Implications for river management and coastal restoration. *Remote Sensing of Environment*, *199*, 39–50. https://doi.org/10.1016/j.rse.2017.06.030

Anthony, E. J., Brunier, G., Besset, M., Goichot, M., Dussouillez, P., & Nguyen, V. L. (2015). Linking rapid erosion of the Mekong River delta to human activities. *Scientific Reports*, *5*(1), 14745. https://doi.org/10.1038/srep14745

Aronoff, S. (1985). The minimum accuracy value as an index of classification accuracy. *Photogrammetric Engineering & Remote Sensing*, *51*(1), 99–111. Retrieved from https://www.asprs.org/wp-content/uploads/pers/1985journal/jan/1985_jan_99-111.pdf

Asensi, A., & Diez-Garretas, B. (2017). Coastal vegetation [Dataset]. *Plant and Vegetation*, 397–432. https://doi.org/10.1007/978-3-319-54867-8_8

Battjes, J. A., & Janssen, J. P. F. M. (1978). Energy loss and set-up due to breaking of random waves. *Coastal Engineering*, *401*, 569–587. https://doi.org/10.1061/9780872621909.03

Beltrán-Burgos, M., Esposito, C. R., Nepf, H. M., Baustian, M. M., & Di Leonardo, D. R. (2023). Vegetation-driven seasonal sediment dynamics in a freshwater marsh of the Mississippi River Delta. *Journal of Geophysical Research: Biogeosciences*, *128*(4). https://doi.org/10.1029/2022JG007143

Besset, M., Anthony, E. J., & Bouchette, F. (2019). Multi-decadal variations in delta shorelines and their relationship to river sediment supply: An assessment and review. *Earth-Science Reviews*, *193*, 199–219. https://doi.org/10.1016/j.earscirev.2019.04.018

Blum, M. D., & Roberts, H. H. (2009). Drowning of the Mississippi Delta due to insufficient sediment supply and global sea-level rise. *Nature Geoscience*, *2*(7), 488–491. https://doi.org/10.1038/ngeo553

Blum, M. J., Rahn, D. A., Frederick, B. C., & Polanco, S. M. (2023). Land loss in the Mississippi River Delta: Role of subsidence, global sea-level rise, and coupled atmospheric and oceanographic processes. *Global and Planetary Change*, *222*, 104048. https://doi.org/10.1016/j.gloplacha.2023.104048

Cahoon, D., Reed, D., Day, J., Lynch, J., Swales, A., & Lane, R. (2020). Applications and utility of the surface elevation table–marker horizon method for measuring wetland elevation and shallow soil subsidence-expansion. *Geo-Marine Letters*, *40*(5), 809–815. https://doi.org/10.1007/s00367-020-00656-6

Cahoon, D. R., Lynch, J. C., Perez, B. C., Segura, B., Holland, R. D., Stelly, C., et al. (2002). High-precision measurements of wetland sediment elevation: II. The rod surface elevation table. *Journal of Sedimentary Research*, *72*(5), 734–739. https://doi.org/10.1306/020702720734

Cahoon, D. R., White, D. A., & Lynch, J. C. (2011). Sediment infilling and wetland formation dynamics in an active crevasse splay of the Mississippi River delta. *Geomorphology*, *131*(3–4), 57–68. https://doi.org/10.1016/j.geomorph.2010.12.002

Chabreck, R. H., & Linscombe, G. (1997). Vegetative type map of the Louisiana coastal marshes [Dataset]. *Louisiana Department of Wildlife and Fisheries*. Retrieved from https://sabdata.cr.usgs.gov/sabnet/priv/net_pub_products/DATA_SPA/2012-16-0003.ZIP

Chadwick, A. J., Steele, S., Silvestre, J., & Lamb, M. P. (2022). Effect of sea-level change on river avulsions and stratigraphy for an experimental lowland delta. *Journal of Geophysical Research: Earth Surface*, *127*(7), e2021JF006422. https://doi.org/10.1029/2021JF006422

Chen, C., Zhang, C., Tian, B., & Zhou, Y. (2022). Satellite observations reveal morphological changes in Asian deltas from 1986 to 2018, ISPRS annals of the photogrammetry, remote sensing and spatial information sciences. *Journal of Spatial Information Science*, *V-3-2022*, 375–381. https://doi.org/10.5194/isprs-annals-V-3-2022-375-2022

Chenevert, E., & Edmonds, D. A. (2024). Machine learning predictions of vertical accretion in the Mississippi River deltaic plain. *Journal of Geophysical Research: Earth Surface*, *129*(3), e2023JF007383. https://doi.org/10.1029/2023JF007383

Coleman, J. M. (1988). Dynamic changes and processes in the Mississippi River delta. *Geological Society of America Bulletin*, *100*(7), 999–1015. https://doi.org/10.1130/0016-7606(1988)100<0999:dcapit>2.3.co;2

Congalton, R. G. (1991). A review of assessing the accuracy of classifications of remotely sensed data. *Remote Sensing of Environment*, *37*(1), 35–46. https://doi.org/10.1016/0034-4257(91)90048-B

Cook, K. L., Turowski, J. M., & Hovius, N. (2020). Width control on event-scale deposition and evacuation of sediment in bedrock-confined channels. *Earth Surface Processes and Landforms: The journal of the British Geomorphological Research Group*, *45*(14), 3702–3713. https://doi.org/10.1002/esp.4993

Couvillion, B. R., Barras, J. A., Steyer, G. D., Sleavin, W., Fischer, M., Beck, H., et al. (2011). *Land area change in coastal Louisiana from 1932–2010* (p. 12). U.S. Geological Survey Scientific Investigations Map 3164, scale 1:265,000. pamphlet. Retrieved from https://pubs.usgs.gov/sim/3164/

Couvillion, B. R., Beck, H., Schoolmaster, D., & Fischer, M. (2017). Land area change in Coastal Louisiana (1932 to 2016). In *Scientific Investigations Map 3381* (p. 16). United States Geological Survey. https://doi.org/10.3133/sim3381

Cox, J. R., Lingbeek, J., Weisscher, S. A. H., & Kleinhans, M. G. (2022). Effects of sea-level rise on dredging and dredged estuary morphology. *Journal of Geophysical Research: Earth Surface*, *127*(10), e2022JF006790. https://doi.org/10.1029/2022JF006790

CRMS. (2022). Marsh surface elevation data [Dataset]. Retrieved from https://www.lacoast.gov/crms_viewer/Map/CRMSViewer

Dai, Z. (2021). Changjiang riverine and estuarine hydro-morphodynamic processes. In *In the Context of Anthropocene Era*. Springer Press. https://doi.org/10.1007/978-981-16-3771-1

Dai, Z. J., Liu, J. T., Wei, W., & Chen, J. Y. (2014). Detection of the three gorges dam influence on the Changjiang (Yangtze River) submerged delta. *Scientific Reports*, *4*(1), 6600. https://doi.org/10.1038/srep06600

Dai, Z. J., Liu, J. T., & Xiang, Y. (2015). Human interference in the water discharge of the Changjiang (Yangtze River), China. *Hydrological Sciences Journal*, *60*(10), 1770–1782. https://doi.org/10.1080/02626667.2014.944182

Day, J. W., Boesch, D. F., Clairain, E. J., Kemp, G. P., Laska, S. B., Mitsch, W. J., et al. (2007). Restoration of the Mississippi delta: Lessons from hurricanes Katrina and Rita. *Science*, *315*(5819), 1679–1684. https://doi.org/10.1126/science.1137030

Day, J. W., Britsch, L. D., Hawes, S. R., Shaffer, G. P., Reed, D. J., & Cahoon, D. (2000). Pattern and process of land loss in the Mississippi delta: A spatial and temporal analysis of wetland habitat change. *Estuaries*, *23*(4), 425–438. https://doi.org/10.2307/1353136

Day, J. W., Twilley, R. R., Freeman, A. M., Couvillion, B. R., Quirk, T., Jafari, N. H., et al. (2023). The concept of land bridge marshes in the Mississippi River delta and implications for coastal restoration. *Nature-Based Solutions*, *3*, 100061. https://doi.org/10.1016/j.nbsj.2023.100061

Dunn, F. E., Darby, S. E., Nicholls, R. J., Cohen, S., Zarfl, C., & Fekete, B. M. (2019). Projections of declining fluvial sediment delivery to major deltas worldwide in response to climate change and anthropogenic stress. *Environmental Research Letters*, *14*(8), 084034. https://doi.org/10.1088/1748-9326/ab304e

Dunn, F. E., & Minderhoud, P. S. J. (2022). Sedimentation strategies provide effective but limited mitigation of relative sea-level rise in the Mekong delta. *Communications Earth & Environment*, *3*(1), 2. https://doi.org/10.1038/s43247-021-00331-3

Edmonds, D. A., Toby, S. C., Siverd, C. G., Twilley, R. R., Bentley, S. J., Hagen, S. C., & Xu, K. (2023). Land loss due to human-altered sediment budget in the Mississippi River Delta. *Nature Sustainability*, *6*(6), 644–651. https://doi.org/10.1038/s41893-023-01081-0

Ericson, J. P., Vörösmarty, C. J., Dingman, L., Ward, L. G., & Meybeck, M. (2006). Effective sea-level rise and deltas: Causes of change and human dimension implications. *Global and Planetary Change*, *50*(1), 63–82. https://doi.org/10.1016/j.gloplacha.2005.07.004

ESA. (2022). Sentinel 2 [Dataset]. *Copernicus*. Retrieved from https://developers.google.com/earth-engine/datasets/catalog/COPERNICUS_S2

Fagherazzi, S. (2008). Self-organization of tidal deltas. *Proceedings of the National Academy of Sciences of the United States of America*, *105*(48), 18692–18695. https://doi.org/10.1073/pnas.0806668105

Fagherazzi, S., Mariotti, G., Leonardi, N., Canestrelli, A., Nardin, W., & Kearney, W. S. (2020). Salt marsh dynamics in a period of accelerated sea level rise. *Journal of Geophysical Research: Earth Surface*, *125*(8), e2019JF005200. https://doi.org/10.1029/2019JF005200

Geleynse, N., Hiatt, M., Sangireddy, H., & Passalacqua, P. (2015). Identifying environmental controls on the shoreline of a natural river delta. *Journal of Geophysical Research: Earth Surface*, *120*(5), 877–893. https://doi.org/10.1002/2014JF003408

Giosan, L., Syvitski, J., Constantinescu, S., & Day, J. (2014). Constantinescu, S. et al. Climate change: Protect the world's deltas. *Nature*, *516*(7529), 31–33. https://doi.org/10.1038/516031a

Google. (2024). Google Earth engine [Platform]. Retrieved from https://code.earthengine.google.com/

Hiatt, M., Snedden, G. A., Day, J. W., Rohli, R. V., Nyman, J. A., Lane, R. R., & Sharp, L. A. (2019). Drivers and impacts of water level fluctuations in the Mississippi River delta: Implications for delta restoration. *Estuarine, Coastal and Shelf Science*, *224*, 117–137. https://doi.org/10.1016/j.ecss.2019.04.020

Hou, W., Liang, S., Sun, Z., Ma, Q., Hu, X., & Zhang, R. (2024). Depositional dynamics and vegetation succession in self-organizing processes of deltaic marshes. *Science of the Total Environment*, *912*, 169402. https://doi.org/10.1016/j.scitotenv.2023.169402

Howes, N. C., FitzGerald, D. M., Hughes, Z. J., Georgiou, I. Y., Kulp, M. A., Miner, M. D., et al. (2010). Hurricane-induced failure of low salinity wetlands. *Proceedings of the National Academy of Sciences of the United States of America*, *107*(32), 14014–14019. https://doi.org/10.1016/j.scitotenv.2023.169402

Jankowski, K., Törnqvist, T., & Fernandes, A. (2017). Vulnerability of Louisiana's coastal wetlands to present-day rates of relative sea-level rise. *Nature Communications*, *8*, 14792. https://doi.org/10.1038/ncomms14792

Jerolmack, D. J. (2009). Conceptual framework for assessing the response of delta channel networks to Holocene sea level rise. *Quaternary Science Reviews*, *28*(17–18), 1786–1800. https://doi.org/10.1016/j.quascirev.2009.02.015

Kumar, P., Dobriyal, M., Kale, A., & Pandey, A. K. (2021). Temporal dynamics change of land use/land cover in Jhansi district of Uttar Pradesh over past 20 years using LANDSAT TM, ETM+ and OLI sensors. *Remote Sensing Applications: Society and Environment*, *23*, 100579. https://doi.org/10.1016/j.rsase.2021.100579

Linscombe, G., & Chabreck, R. (2006). Task III.8—Coastwide aerial survey, Brown marsh 2001 assessment: Salt marsh dieback in Louisiana—Brown marsh data information management system [Dataset]. Retrieved from http://sabdata.cr.usgs.gov/sabnet/priv/net_pub_products/DATA_SPA/2012-16-0002.ZIP

Mei, X. F., Dai, Z. J., van Gelder, P. H. A. J. M., & Gao, J. J. (2015). Linking three gorges dam and downstream hydrological regimes along the Yangtze River, China. *Earth and Space Science*, *2*(4), 94–106. https://doi.org/10.1002/2014EA000052

Nardin, W., & Edmonds, D. A. (2014). Optimum vegetation height and density for inorganic sedimentation in deltaic marshes. *Nature Geoscience*, *7*(10), 722–726. https://doi.org/10.1038/ngeo2233

Nardin, W., Edmonds, D. A., & Fagherazzi, S. (2016). Influence of vegetation on spatial patterns of sediment deposition in deltaic islands during flood. *Advances in Water Resources*, *93*, 236–248. https://doi.org/10.1016/j.advwatres.2016.01.001

Nienhuis, J. H., Ashton, A. D., Edmonds, D. A., Hoitink, A. J. F., Kettner, A. J., Rowland, J. C., & Törnqvist, T. E. (2020). Global-scale human impact on delta morphology has led to net land area gain. *Nature*, *577*(7791), 514–518. https://doi.org/10.1038/s41586-019-1905-9

Nienhuis, J. H., Kim, W., Milne, G. A., Quock, M., Slangen, A. B. A., & Törnqvist, T. E. (2023). River deltas and sea-level rise. *Annual Review of Earth and Planetary Sciences*, *51*(1), 79–104. https://doi.org/10.1146/annurev-earth-031621-093732

NOAA. (2015). Southern Louisiana 1/3 arc-second NAVD 88 coastal digital elevation model [Dataset]. *NOAA*. Retrieved from https://www.ncei.noaa.gov/access/metadata/landing-page/bin/iso?id=gov.noaa.ngdc.mgg.dem:1521

NOAA. (2021). Wave direction and significant wave height at the buoy 42040 [Dataset]. *NOAA*. Retrieved from https://www.ndbc.noaa.gov/station_history.php?station=42040

NOAA. (2022). Relative sea level trend at 8761724 Grand Isle [Dataset]. *Louisiana*. Retrieved from https://tidesandcurrents.noaa.gov/waterlevels.html?id=8761724

Nyman, J. A., Reid, C. S., Sasser, C. E., Linscombe, J., Hartley, S. B., Couvillion, B. R., & Villani, R. K. (2022). Vegetation types in coastal Louisiana in 2021 (ver. 2.0, April 2023): US Geological Survey data release [Dataset]. https://doi.org/10.5066/P9URYLMS

Olson, K. R., & Suski, C. D. (2021). Mississippi River delta: Land subsidence and coastal erosion. *Open Journal of Soil Science*, *11*(3), 139–163. https://doi.org/10.4236/ojss.2021.113008

Overeem, I., & Syvitski, J. P. M. (2009). *Dynamics and vulnerability of delta systems. Technical Report 35* (p. 54). LOICZ Reports & Studies. GKSS Research Center. https://doi.org/10.13140/RG.2.1.5183.6644

Paola, C. (2016). A mind of their own: Recent advances in autogenic dynamics in rivers and deltas. In D. A. Budd, E. A. Hajek, & S. J. Purkis (Eds.), *Autogenic Dynamics and Self-Organization in Sedimentary Systems* (Vol. 106, pp. 5–17). SEPM Society for Sedimentary Geology. https://doi.org/10.2110/sepmsp.106

Penland, S., Wayne, L., Britsch, L., Williams, S., Beall, A., & Butterworth, V. (2000). *Process classification of coastal land loss between 1932 and 1990 in the Mississippi River Delta plain, southeastern Louisiana*. U.S. Geological Survey Open File Report 00: U.S. Geological Survey Open File Report 00–418. https://doi.org/10.3133/ofr00418

Sasser, C. E., Visser, J. M., Mouton, E., Linscombe, J., & Hartley, S. B. (2008). Vegetation types in coastal Louisiana in 2007 [Dataset]. *U.S. Geological Survey Open-File Report 2008–1224, 1 sheet, scale 1:550,000*. Retrieved from https://pubs.usgs.gov/of/2008/1224/

Sasser, C. E., Visser, J. M., Mouton, E., Linscombe, J., & Hartley, S. B. (2014). Vegetation types in coastal Louisiana in 2013 [Dataset]. *U.S. Geological Survey Scientific Investigations Map 3290, 1 sheet, scale 1:550,000*. https://doi.org/10.3133/sim3290

Schuerch, M., Spencer, T., Temmerman, S., Kirwan, M. L., Wolff, C., Lincke, D., et al. (2018). Future response of global coastal wetlands to sea-level rise. *Nature*, *561*(7722), 231–234. https://doi.org/10.1038/s41586-018-0476-5

Syvitski, J. P., & Saito, Y. (2007). Morphodynamics of deltas under the influence of humans. *Global and Planetary Change*, *57*(3–4), 261–282. https://doi.org/10.1016/j.gloplacha.2006.12.001

Twilley, R. R., Day, J. W., Bevington, A. E., Castañeda-Moya, E., Christensen, A., Holm, G., et al. (2019). Ecogeomorphology of coastal deltaic floodplains and estuaries in an active delta: Insights from the Atchafalaya Coastal Basin. *Estuarine, Coastal and Shelf Science*, *227*, 106341. https://doi.org/10.1016/j.ecss.2019.106341

USGS. (2011). Landsat 5 surface reflectance tier 1 level-2 collection 2 (LANDSAT/LT05/C02/T1_L2) [Dataset]. *U.S. Geological Survey*. Retrieved from https://developers.google.com/earth-engine/datasets/catalog/LANDSAT_LT05_C02_T1_L2

USGS. (2019). Landsat 8 surface reflectance tier 1 level-2 collection 2 (LANDSAT/LC08/C02/T1_L2) [Dataset]. *U.S. Geological Survey*. Retrieved from https://developers.google.com/earth-engine/datasets/catalog/LANDSAT_LC08_C02_T1_L2

USGS. (2021). USGS 07295100 Mississippi River at Tarbert landing, MS [Dataset]. Retrieved from https://waterdata.usgs.gov/nwis/inventory?agency_code=USGS&site_no=07295100

Wells, J. T., & Coleman, J. M. (1987). Wetland loss and the subdelta life cycle. Estuarine. *Coastal and Shelf Science*, *25*(1), 111–125. https://doi.org/10.1016/0272-7714(87)90029-1

Whitbread, K., Jansen, J., Bishop, P., & Attal, M. (2015). Substrate, sediment, and slope controls on bedrock channel geometry in postglacial streams. *Journal of Geophysical Research: Earth Surface*, *120*(5), 779–798. https://doi.org/10.1002/2014JF003295

White, D. A. (1993). Vascular plant community development on mudflats in the Mississippi River delta, Louisiana, USA. *Aquatic Botany*, *45*(2–3), 171–194. https://doi.org/10.1016/0304-3770(93)90020-W

Yang, H. F., Yang, S., Li, B. C., Wang, Y. P., Wang, J. Z., Zhang, Z. L., et al. (2021). Different fates of the Yangtze and Mississippi deltaic wetlands under similar riverine sediment decline and sea-level rise. *Geomorphology*, *381*, 107646. https://doi.org/10.1016/j.geomorph.2021.107646

Zhang, X., Xu, K., Yang, Z., Tan, X., & Wu, C. (2021). Decreasing land growth and unique seasonal area fluctuations of two newborn Mississippi subdeltas. *Geomorphology*, *378*(1), 107617. https://doi.org/10.1016/j.geomorph.2021.107617

References From the Supporting Information

Huete, A., Didan, K., Miura, T., Rodriguez, E. P., Gao, X., & Ferreira, L. G. (2002). Overview of the radiometric and biophysical performance of the MODIS vegetation indices. *Remote Sensing of Environment*, *83*(1–2), 195–213. https://doi.org/10.1016/S0034-4257(02)00096-2

Rouse, J. W., Haas, R. H., Scheel, J. A., & Deering, D. W. (1974). Monitoring vegetation systems in the Great Plains with ERTS. *Proceedings, 3rd Earth Resource Technology Satellite (ERTS) Symposium*, *1*, 48–62. Retrieved from https://ntrs.nasa.gov/citations/19740022614

Xu, H. (2006). Modification of normalized difference water index (NDWI) to enhance open water features in remotely sensed imagery. *International Journal of Remote Sensing*, *27*(14), 3025–3033. https://doi.org/10.1080/01431160600589179